ELSEVIER

Contents lists available at ScienceDirect

Mechanics Research Communications

journal homepage: www.elsevier.com/locate/mechrescom





Multiwalled carbon nanotubes as hard templates to yield advanced geopolymer-based self-assembled nanostructured ceramics

Yunzhi Xu^a, Haklae Lee^a, Nathanial Buettner^a, Ange-Therese Akono^{a,b,*}

- a Department of Civil and Environmental Engineering, Northwestern University, IL 60208, USA
- ^b Department of Mechanical Engineering, Northwestern University, IL 60208, USA

ARTICLE INFO

Keywords:
Geopolymer
Self-assembled materials
Multiwalled carbon nanotubes
Nanostructured ceramics

ABSTRACT

Novel multifunctional construction materials are needed to promote resilient infrastructure in the face of climate change and extreme weather. Nanostructured materials such as geopolymer reinforced with carbonbased nanomaterials are a promising way to reach that goal. In recent years, several studies have investigated the influence of nanomaterials on the physical properties of geopolymer composites such as compressive strength and fracture toughness. Yet, a fundamental understanding of the influence of nanomaterials on the nanoscale and micron-scale structure has been elusive so far. Our research objective is to understand how multiwalled carbon nanotubes (MWCNT) can help tailor the microstructure of geopolymers to yield architected multifunctional nanocomposites. We synthesized geopolymer nanocomposites reinforced with 50-nm thick multiwalled carbon nanotubes with mass fractions in the range of 0.1 wt%, 0.2 wt%, and 0.5 wt%. Our major finding is that MWCNTs act as hard templates that promote geopolymer formation via self-assembly. Geopolymer nanoparticle growth is observed along the walls of MWCNTs. A refinement in grain size is observed: increasing the fraction of MWCNTs by 0.5 wt% leads to a reduction in grain size by 54%. Similarly, increasing the mass fraction of MWCNTs leads to a densification of the geopolymer matrix as demonstrated by the Fourier transform infrared spectroscopy results and the statistical deconvolution analysis. Mercury intrusion porosimetry shows a nanoscale tailoring of the pore size distribution: a 26% decrease in porosity is observed as the fraction of MWCNTs is increased to 0.5 wt%. As a result of these nanoscale structural changes, a greater resistance to long-term deformation is observed for MWCNT-reinforced geopolymers, as the creep modulus increases both locally and macroscopically. At the macroscopic level, a 42% increase in the macroscopic logarithmic creep modulus is observed as the fraction of MWCNTs is increased to 0.5 wt%. These findings and the supporting methodology are important to understand how to manipulate matter below 100 nm. This research also paves the way for the design of resilient infrastructure materials with tailored microstructure and mechanical properties.

1. Introduction

New civil engineering materials are needed to promote resilience in the face of climate change and extreme weather [1]. In that aspect, novel construction materials are required to be multifunctional: durable, tough, lightweight, and with enhanced mechanical properties. One way to achieve this great demand for multifunctionality is through architecting the structure at the nanoscale by focusing on nanostructured materials. Nanostructured materials are typically defined as materials composed of structural elements, such as clusters, crystallites, or molecules, with dimensions ranging from 1 to 100 nanometers [2]. These materials exhibit unique properties that arise from their nanoscale size and extremely high surface-to-volume ratio,

which bring distinct behavior that is absent in their bulk counterparts. The extraordinary properties of nanostructured materials include increased surface reactivity [3,4] and improved mechanical strength [5,6], making nanostructured materials highly desirable for a wide range of applications, such as electronics [7,8], catalysis [9–11], energy storage and conversion [3,4], drug delivery [12,13], environmental remediation [14,15], and composite manufacturing [16,17].

An example of nanostructured materials is geopolymer. Geopolymer is a covalently bonded ceramic material that is X-ray amorphous, nanoporous and nanoparticulate with a grain size less than 15 nm [18–20]. The formation of the geopolymer matrix can be described as a self-assembly process that occurs in two steps: (i) the preceramic precursor of geopolymer self-aggregates into macromolecules arranged in

^{*} Correspondence to: TECH A132 2145 Sheridan Road, Evanston, IL 60208, USA. E-mail address: ange-therese.akono@northwestern.edu (A.-T. Akono).

Table 1
Mixture design of Multi-walled carbon nanotubes (MWCNT) reinforced geopolymer composites. The dispersion energy is the dispersion energy provided initially to disperse the MWCNTs using an ultrasonic probe.

Sample name	Nanomaterial	Fiber fraction	Dispersion Energy
CNT-0.1	MWCNT	0.1 wt%	8 kJ
CNT-0.2	MWCNT	0.2 wt%	16 kJ
CNT-0.5	MWCNT	0.5 wt%	160 kJ

micelles [21,22]; (ii) upon curing, the micelles, which form a colloidal suspension, go through irreversible covalent bonding assisted [23,24] and capillary force assisted [25,26] self assembly, resulting in a spongelike or nanoporous ceramic matrix [27]. In terms of civil infrastructure, some applications of geopolymer include green cement [28], structure repair [29], and chemical-resistant coatings [30].

Recent advances in geopolymer research have been focusing on incorporating carbon-based nanomaterials into geopolymers to produce performance-enhanced geopolymer nanocomposites [31]. An increase in compressive strength has been reported for geopolymer reinforced with MWCNTs [32,33] and the underlying mechanisms were porosity refinement [33] and crack bridging [32]. Chen and Akono [5] incorporated multiwalled carbon nanotubes (MWCNTs) in geopolymer at concentrations ranging from 0.3 wt% to 1.5 wt%, and demonstrated densification of the microstructure of geopolymer and an increase in stiffness and fracture toughness induced by MWCNTs. Akono [6] adopted scratch testing to characterize the fracture toughness of carbon nanofiber (CNF)-reinforced geopolymer and reported that CNFs can enhance the fracture toughness of metakaolin-based geopolymer by up to 45% at a concentration of 0.5 wt% through crack bridging mechanisms. However, the focus has been primarily on maximizing macroscopic properties such as compressive strength, flexural strength, and fracture toughness and little emphasis has been given to designing the nanostructure to yield nanocomposites with tailored properties.

In brief, most works on nanoreinforced geopolymers have focused on improvements in macroscopic properties. Yet, few studies have been performed to investigate the influence of carbon-based nanomaterials on the nanoscale architecture of geopolymer materials. In this study, we seek to understand the influence of nanomaterials on the nanoscale and micron-scale structure. Our research hypothesis is that multi-walled carbon nanotubes (MWCNTs) will serve as hard templates to facilitate the self-assembly process of geopolymer nanocomposites. To this end, we perform a comprehensive characterization at the nanoscale to investigate the effect of MWCNTs on the microstructure, chemical structure, pore structure, and viscoelastic mechanical properties of geopolymer materials. The end goal is to gain insights into the effect of MWCNTs on the material architecture at the nanoscale, and to contribute to future design and manufacturing of multifunctional self-assembled nanostructured civil engineering materials.

2. Materials and methods

2.1. Materials

Metakaolin-based geopolymer nanocomposites were synthesized with multiwalled carbon nanotubes (MWCNTs), and with the values of the mass fraction %wt per 100 g of composite, % wt = 0.1, 0.2, 0.5, see Table 1. The reference material had a chemical formula $K_2O\cdot Al_2O_3\cdot 4SiO_2\cdot 11H_2O$, and consisted of 55.22 g of deionized water, 36.86 g of fumed silica (Wacker, Munich, Germany), 39.74 g of potassium hydroxide (Thermo Fisher Scientific, Waltham, MA, USA), and 68.16 g of metakaolin. We used synthetic metakaolin (MetataMax from BASF Corporation), that is a high-reactivity calcined metakaolin with a particle size of 70 nm, and a surface area of 300 m^2/g . The multiwalled carbon nanotubes used in this study (Cheaptubes, Grafton, VT,

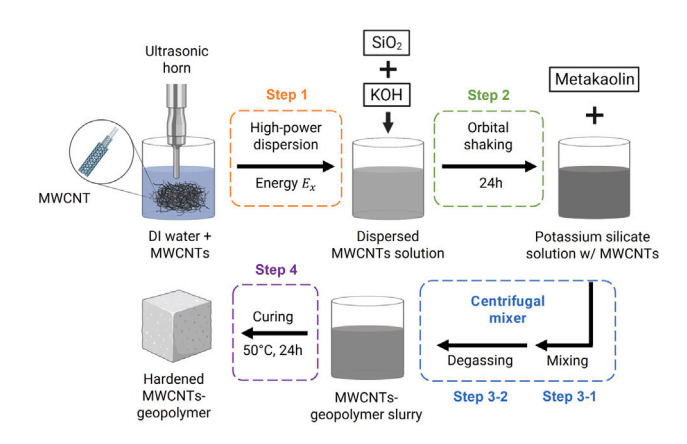


Fig. 1. Schematic of synthesis protocol of MWCNT-reinforced metakaolin-based geopolymer.

USA) were tubular with an outer diameter of 50-80 nm, a length of 10-20 μ m, and a specific surface area of 60 m²/g.

The synthesis of ceramic nanocomposites occurred in a four-step process which is illustrated in Fig. 1. Step 1: 2 × %wt g of nanomaterials were dispersed in 55.22 g of deionized water, where %wt is the mass fraction of nanomaterial per 100 g of nanocomposite. The nanomaterials were dispersed using a VCX 750 (Sonic & Materials Inc, Newton, CT, USA) ultrasonic probe. Step 2: the waterglass was mixed using the mixture of nanomaterials dispersed in deionized water along with 36.86 g of fumed silica, and 39.74 g of potassium hydroxide. The waterglass was then aged for 24 h under continuous stirring at 100 rpm speed. Step 3: the nanocomposite geopolymer slurry was mixed by adding 68.16 g of synthetic metakaolin to the waterglass using a planetary centrifugal mixer THINKY ARE 310 (THINKY USA, Laguna Hills, CA, USA). This third step involved two stages: centrifugal mixing, and then degassing. The mixing speed and mixing time for centrifugal mixing were (3 min, 1200 rpm), (3 min, 1200 rpm), (3 min, 1300 rpm), and (4 min, 1400 rpm), respectively for the reference sample, 0.1 wt% sample, 0.2 wt%, and 0.5 wt% sample. Meanwhile, the mixing speed and mixing time for degassing were (3 min, 1400 rpm), (3 min, 1400 rpm), (3 min, 1500 rpm), and (5 min, 1600 rpm), respectively for the reference sample, 0.1 wt% sample, 0.2 wt%, and 0.5 wt% sample. Step 4: the samples were cast into plastic molds, wrapped with polyethylene films to limit water evaporation, and cured in an incubator at 50 °C for 24 h while continuously stirring at 100 rpm.

2.2. Methods

2.2.1. Grinding and polishing

Prior to nanoscale microscopy analyses and mechanical tests, grinding and polishing was performed to yield flat and polished surfaces. First, the samples were embedded using a low-viscosity epoxy resin and then cut into 5-mm thick slices with a low-speed diamond saw. The 5-mm thick slices were mounted on 35-mm aluminum disks using a cyanoacrylate adhesive. Grinding was performed with a semi-automated Automet $^{\circledR}$ 250/ Ecomet $^{\circledR}$ 300 (Buehler, Lakebluff, IL, USA) polisher using silicon carbide pads of grit size consecutively 240, 400, 600, and 800. Polishing was performed using Microcloth $^{\circledR}$ (Buehler, Lakebluff, IL, USA) polishing cloths along with polycrystalline diamond suspensions of particle size consecutively 1 μm , and 0.25 μm . In between each grinding and polishing step, the samples were rinsed for two minutes using an ultrasonic cleaner with N-decane being the cleaning solution. Afterwards, the samples were stored in a vacuum dessicator awaiting for further testing.

2.2.2. Scanning Electron Microscopy (SEM)

The characterization of the microstructure of MWCNT-reinforced geopolymer nanocomposites was conducted using a Quanta 650 environmental scanning electron microscope (FEI, Hillsboro, OR, USA). Prior to SEM analysis, the polished geopolymer specimens were rinsed in an inert oil-based solvent and cleaned using ultrasonic energy for 2 min to eliminate surface contamination. Due to the low conductivity of geopolymer materials, a low vacuum mode with an accelerating voltage of 15.00 kV was used for the entire analysis procedures. The secondary electron detector was selected under the following operation conditions: a chamber pressure of 0.53 Torr, a working distance of 6.0 mm, a spot size of 6.0, and an aperture of 4.

2.2.3. Transmission Electron Microscopy (TEM)

An analytical scanning transmission atomic resolution electron microscope (JEM-2100 FasTEM, JEOL, Tokyo, Japan) was employed for structural analysis and qualitative micro-porosity observations. Preparation of thin geopolymer samples (less than a thickness of 500 nm) for TEM analysis is extremely difficult due to the presence of numerous cracks crossing the specimens. Powder samples of the prepared specimens were used instead. For this purpose, bulk geopolymer samples were milled with ethanol using an XRD-Mill (McCrone, Westmont, IL, USA) to generate powder specimens; the ethanol served as a coolant. The powdered geopolymer specimens were then temporarily dispersed in ethanol using ultrasonic energy for 2 min and deposited on the TEM grid (Formvar/Carbon 200 mesh, Copper). The pure MWCNT samples as purchased were dispersed in ethanol and deposited on the TEM grid. Single tilt holder was selected for mounting the TEM grid and the TEM was operated at 200 kV.

To obtain a quantitative analysis of the microstructure of MWCNTreinforced geopolymer composites, digital image analysis based on the TEM images were carried out using ImageJ to investigate the grain size in the geopolymer composites. ImageJ is commonly combined with TEM analysis to study the particle size of nanocomposites [34-36]. In this study, the image analysis involves several steps. First, the TEM image was cropped to a 100 nm × 100 nm region of interest (ROI) that effectively highlighted the grain structures. Then, a threshold of the ROI's histogram of the grey-scale values was identified to isolate the grains from the background. Next, the 'Smooth' function was applied to smooth the rough boundaries of the grains to improve their recognition in composite matrices. The particle analysis was performed with a maximum limit of 100 nm² for the areal grain size to filter out overlyaggregated and large matrix areas. Finally, the size distribution of the grains was plotted based on the exported grain size data. The details of image analysis can be found in the Supplementary Materials.

2.2.4. Powder X-ray diffraction analysis

Powder X-ray diffraction (XRD) analysis was conducted to investigate the chemical characteristics of geopolymer composites. Before XRD testing, the bulk samples were ground into powders and refined using an XRD-Mill (McCrone, Westmont, IL, USA) to a final fineness of less than 1 μ m. Wet ball milling using a McCrone Mill is a standard preparation procedure of samples for powder X-ray analysis [37,38]. XRD diffractograms were collected using an automated X-ray diffractometer (Ultima IV, Rigaku, Tokyo, Japan) equipped with a CuK α source ($\lambda = 1.5406$ nm). The powder samples were scanned at 40 kV, 30 mA, and at Bragg angles (2θ) ranging from 5° to 70°. The scan speed was 0.5°/min, and the step size was 0.1° [39]. Phase identification of the samples was performed using Jade software via whole pattern fitting of X-ray data [40].

2.2.5. Fourier-Transform Infrared Spectroscopy

Fourier-Transform Infrared Spectroscopy (FTIR) was performed by a Nicolet iS50 FTIR spectrometer (Thermo Fisher Scientific, Waltham, MA, USA) using the transmission sampling technique. KBr powder was mixed with the sample powder at a weight ratio of 100:1. The powder mixture was then pressed into pellets for FTIR testing. The FTIR spectra was recorded in absorption mode from 4000 $\rm cm^{-1}$ to 400 $\rm cm^{-1}$ at a resolution of 4 $\rm cm^{-1}$ and 64 scans per spectrum.

2.2.6. Mercury intrusion porosimetry

Mercury intrusion porosimetry (MIP) is a standard method for pore structure assessment of cement-based materials [41–43] and in this study, it was utilized to investigate the pore structures of the potassium geopolymers. The potassium geopolymers were prepared for MIP testing by first cutting the bulk material into 3-mm prismatic pieces using the Techcut 4 precision diamond saw (Allied High Tech Products, Inc, Compton, CA, USA) with N-decane as the cutting fluid. Then, approximately 1 g of each material was collected to create powder samples. The powder samples were placed in an oven at 50 °C for 24 h prior to testing to evaporate moisture from the pore structure. The MIP testing was performed using an Autopore V (Micromeritics, Norcross, GA, USA). The testing protocol consisted of a low-pressure analysis from 0–345 kPa and a high-pressure analysis from 345 kPa-228 MPa, resulting in mercury intrusion porosimetry measurements at mean pore diameters between 5.6 nm and 179 μ m.

The MIP data was used to estimate the porosity, bulk density, skeletal density, and water permeability of the potassium geopolymers. To calculate the water permeability, the intrinsic permeability was first calculated using the Katz–Thompson equation [44]:

$$k = \frac{1}{89} d_{max}^2 (d_{max}/d_{char}) I_{tot} Y_b S_{d_{max}}$$
 (1)

where k is the intrinsic permeability (m²), d_{max} is the pore diameter corresponding to the maximum hydraulic conductance (m), d_{char} is the characteristic pore diameter (m), I_{tot} is the total specific intrusion volume (mL/g), Y_b is the bulk density (g/cm³), and $S_{d_{max}}$ is the fractional volume of connected pore spaces involving pore diameters d_{max} and larger. In this study, the characteristic pore diameter was taken as the threshold pore diameter. For each test, the threshold pore diameter was calculated using the method that Ma suggested for cement-based materials [43]. In other words, the threshold pore diameter was found as the intersection point of two linear trendlines that represent the linear portions of the cumulative intrusion volume curve obviously before and after the threshold pore diameter. The pore diameter d_{max} was found to be where the quantity, $(I-I_{thr})d^3$ is a maximum, in which I is the specific intrusion volume corresponding to pore diameter d and I_{thr} is the specific intrusion volume corresponding to the threshold pore diameter.

With the intrinsic permeability k, the water permeability was then calculated with the following equation:

$$K = k \frac{\rho_w g}{\eta} \tag{2}$$

where k is the intrinsic permeability (m²), ρ_w is the density of water (kg/m³), g is the gravitational acceleration (m²/s), and η is the dynamic viscosity of water (Ns/m²). The properties of water at 20 °C were assumed.

2.2.7. Creep indentation testing

The viscoelastic properties were measured using creep indentation testing. In our experiments, a Berkovitch indenter was pushed against the surface of the material while recording the corresponding increase in penetration depth. All tests were performed using an Anton Paar Nanohardness Tester NHT 2 with a load resolution of 300 nN and a depth resolution of 0.06 nm. The prescribed vertical load history was trapezoidal with a maximum vertical force of 2 mN, a loading/unloading rate of 4 mN/min, and a holding period of 30 s. The Oliver & Pharr model [45] was applied to compute the initial plane strain indentation modulus M_0 and the indentation hardness H from, respectively, the initial slope at unloading S and the maximum penetration depth h_{max} according to:

$$E_r = \frac{\sqrt{\pi}}{2} \frac{A}{\sqrt{A}}; \quad H = \frac{P_{\text{max}}}{A(h_{\text{max}})}$$
 (3)

with

$$\frac{1}{E_r} = \frac{1}{M_{ind}} + \frac{1}{M_0} \tag{4}$$

Here M_{ind} is the plane strain elastic modulus of the diamond indenter $(M_{ind}=1093~{\rm GPa})$, and A(h) is the indenter contact area function.

The viscoelastic properties were computed using nonlinear viscoelastic solutions for indentation [46,47]. In particular, the contact creep compliance $\dot{L}(t)$ is given by [46,47]:

$$\dot{L}(t) = \frac{2a_U \dot{h}(t)}{P_{\text{max}}} \tag{5}$$

where a_U is the contact radius upon unloading, $\dot{h}(t)$ is the rate of change in penetration depth during the holding phase, and $P_{\rm max}$ is the prescribed maximum vertical force. The contact creep compliance function is modeled using a logarithmic function:

$$L(t) = \frac{1}{M_0} + \frac{1}{4C} \ln\left(1 + \frac{t}{\tau}\right)$$
 (6)

With C being the contact creep modulus and τ being the logarithmic creep characteristic time.

2.3. Statistical deconvolution

We conducted high-throughput creep indentation tests to map the spatial heterogeneity of the mechanical properties. For each specimen, we used a 11×11 indentation grid, resulting in 121 individual indentation tests. The spacing between indents was 20 µm so that each indentation grid covered an area of 200 $\mu m \times 200$ μm . Afterward, we employed statistical deconvolution, which is a clustering method aiming to represent a distribution as the weighted sum of individual Gaussian functions. The design space involved four variables: (M_0, H, C, τ) , where M is the indentation modulus, H is the indentation hardness, C is the logarithmic creep, τ is the logarithmic creep characteristic time. For each individual indentation test, all four coefficients are locally computed using Eqs. (5)-(6). A custom-written statistical deconvolution algorithm written in Python was used to identify microconstituent characteristics of each nanocomposites from the distribution $\left(M_{0i},H_i,C_i, au_i\right)_{1\leq i\leq 121}$. The basic concept is to employ a Gaussian mixture modeling approach to decompose a full distribution as weighted sum of individual Gaussian functions [48,49]. We prescribed a phase separability criterion to prevent any significant overlap between neighboring phases. We also applied a Bayesian information criterion to determine the optimum number of phases [50].

Using a multiscale approach, we estimated the macroscopic creep modulus from the individual measurements $C_{i,1 \le i \le 121}$ using micromechanical solutions for heterogeneous viscous solids [47]:

$$\sum_{i=1}^{N} \frac{1}{1 + \frac{1}{2} \left((C_i/C^{hom}) - 1 \right)} = \sum_{i=1}^{441} \frac{C_i/C^{hom}}{1 + \frac{1}{2} \left((C_i/C^{hom}) - 1 \right)}$$
 (7)

where N is the total number of indentation tests per indentation grid (N=441). We solved Eq. (7) using a recursive algorithm written in Python.

3. Results

3.1. Microstructural characteristics

The microstructures of the MWCNT-reinforced geopolymer nanocomposites are shown in Fig. 2. Through SEM analysis, the MWC-NTs are clearly identified in the geopolymer matrix. The MWCNTs in geopolymer matrices tend to be found located inside the pores formed on the specimen surfaces. These findings agree with Chen and Akono [5] and Ahmadi et al. [51]who found that MWCNTs fill micropores. The sizes of the pores appear to be less than 5 μm . The MWCNTs are found to be integrated with the geopolymer particles, as displayed in the pores. This bonding between the MWCNTs and the geopolymer nanoparticulates in the pores may result in a reduction of the porosity of the geopolymer composites. To further characterize the morphology of embedded MWCNTs in the geopolymer matrices, a

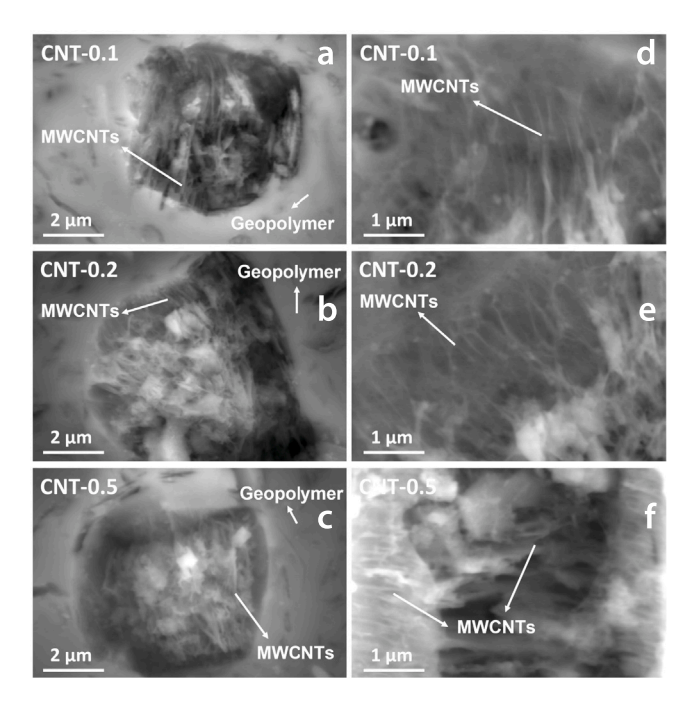


Fig. 2. SEM images of MWCNT-reinforced geopolymer composites: (a, b, and c) $20,000\times$ magnification; (d, e, and f) $40,000\times$ magnification.

higher magnification level (40000×) was attempted to acquire highresolution SEM images. From the results, the embedded MWCNTs are located on the walls of the pores, as well as bridging the microcracks present in the hardened geopolymer matrix, suggesting a toughening mechanism induced by the MWCNTs. Moreover, the average diameters of the MWCNTs shown in the SEM images are measured as approximately 50 nm, which is in consistent with the specification of the purchased MWCNTs.

The high-resolution TEM images are shown in Fig. 3. Geopolymer nanoparticles growth is observed along the walls of MWCNTs. The MWCNT-reinforced geopolymer composites display a sponge-like structure with compact nanoporosity over the surfaces of powdered geopolymer composites (Fig. 3a). These microstructures are in good agreement with previously reported results by Kriven et al. [27,40] and Duxson et al. [52]. Image analysis was performed to study the grain size of the geopolymer composites based on the TEM images. Average areal grain sizes are measured to be 7.28, 4.08, 3.42 and 3.33 nm² for pure KGP, CNT-0.1, CNT-0.2, and CNT-0.5 samples, respectively. With the increase of the concentration of MWCNTs in the geopolymer composites, a decrease in the grain size of the composites is observed, which can lead to a potential increase of grain packing density in the material. The details of image analysis and grain size distributions of the geopolymer composites are provided in the Supplementary Materials document. On the other hand, the presence of embedded MWCNTs is also evident from TEM analysis of powdered geopolymer specimens (Fig. 3b). The diameters of MWCNTs agree with those shown in SEM images, suggesting a homogeneous dispersion of the MWCNTs. Meanwhile, geopolymer nanoparticulates tend to nucleate along the MWCNTs. Moreover, the dispersed MWCNTs form a network within the bulk reaction space and act as a hard template [53,54] for the geopolymerization reaction, therefore, templating the nanoscale structure of final geopolymer composites.

3.2. Chemical characteristics

Compared to pure KGP, MWCNTs improve the interaction between the reactive materials by shifting the amorphous hump of geopolymer

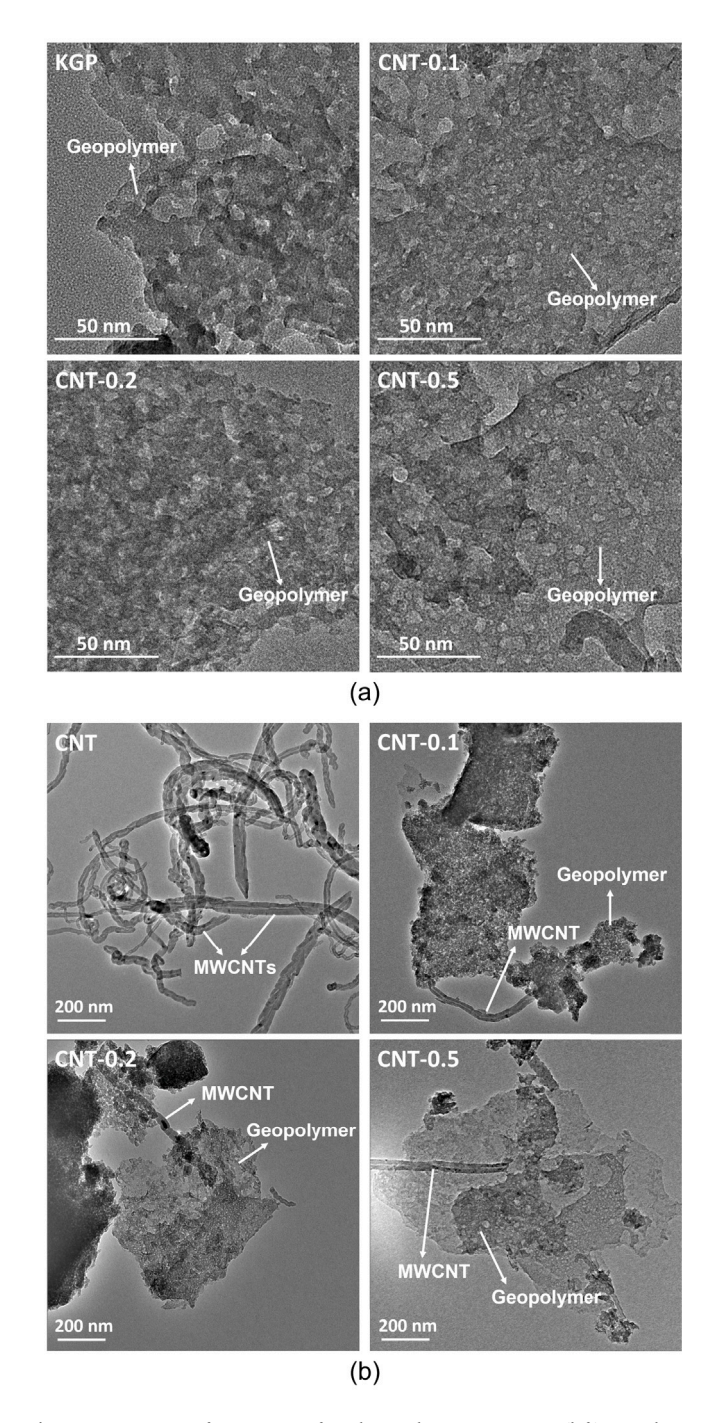


Fig. 3. TEM images of MWCNT-reinforced geopolymer composites: (left) geopolymer particles; (right) MWCNTs in geopolymer matrices.

materials towards a higher value. Fig. 4 displays the XRD diffractograms of the geopolymer composites reinforced with MWCNTs in comparison with synthetic metakaolin and pure KGP. Research has demonstrated that geopolymers resulting from the polycondensation of alkali-alumino-silicates are X-ray amorphous [55]. MWCNTs preserve the amorphous nature of geopolymers. The metakaolin used in this study contains small amount of anatase impurity, shown as the peaks at 25°, 38°, 48°, 54°, 55°, and 63° sustained in all the X-ray patterns of the samples. For pure geopolymer, the characteristic amorphous hump centers at 27.5°. For MWCNT-reinforced geopolymer composites, this hump centers at 27.5°, 28.0°, 27.8° for 0.1 wt%, 0.2 wt%, and 0.5 wt% of MWCNTs, respectively. Our findings agree with Zidi et al. [56] who

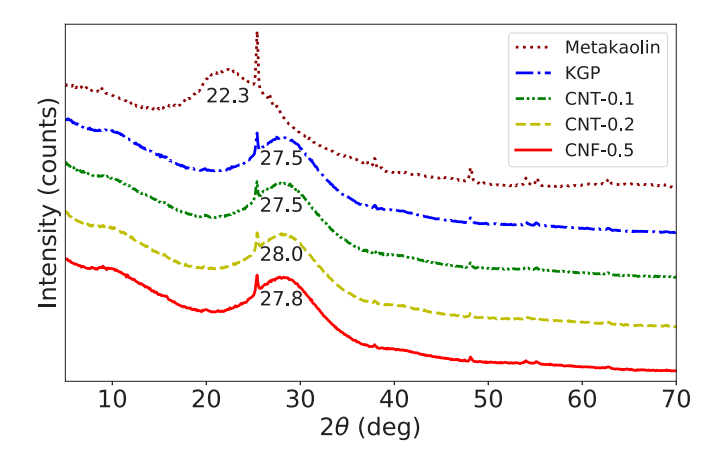


Fig. 4. XRD diffractograms of metakaolin, pure geopolymer (KGP) and MWCNT-reinforced geopolymer composites.

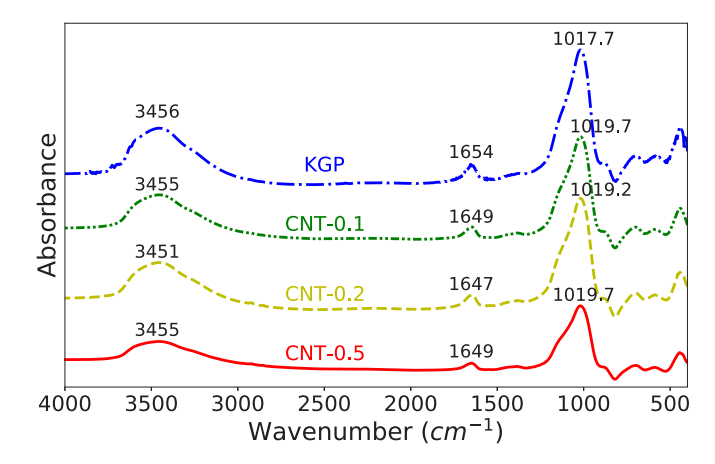


Fig. 5. FTIR spectra of pure geopolymer (KGP) and MWCNT-reinforced geopolymer composites.

found that the addition of nanosilica promoted geopolymer growth: here, a similar result is observed with MWCNTs. Among the three composite samples, CNT-0.2 exhibits the largest hump center location. This observation points to a change in the chemical lattice structure of the geopolymer composites, which was further examined by the FTIR analysis.

The FTIR spectra of MWCNT-reinforced geopolymer composites are displayed in Fig. 5, along with that of KGP. From FTIR analysis, the incorporation of MWCNTs facilitates the formation of a denser structure in the geopolymer composites. The peaks at approximately 3455 cm⁻¹ and 1650 cm⁻¹ in the spectra were assigned to stretching and bending vibration of free H₂O [57]. The primary focus of analyzing geopolymer materials is the "main band" identified between 1200-900 cm⁻¹, which corresponds to the asymmetric stretching of Si-O-Si(Al) bonds [58]. For pure KGP, the peak of the main band is at the wavenumber of $1017.7~\mbox{cm}^{-1}$. In MWCNT-reinforced geopolymer composites, the main band peaks at 1019.7 cm⁻¹ for CNT-0.1, 1019.2 cm⁻¹ for CNT-0.2 and $10\overline{19.7}$ cm $^{-1}$ for CNT-0.5. This shift of frequency towards a larger wavenumber can be related to the shortening of the Si-O-Si(Al) bond and increase in the bond angle, which indicates a denser structure formed by adding the MWCNTs [59]. These findings agree with Ahmadi et al. [51] who reported a shift in the geopolymer main band after addition of MWCNTs into metakaolin-red mud geopolymer. The intensity of the main band is lower with higher weight fraction of MWCNTs, which points to a smaller concentration of the Si-O-Si(Al) bond. This is due to the higher volume fraction of MWCNTs present in the composite materials. In addition, the intensity of the hydroxyl

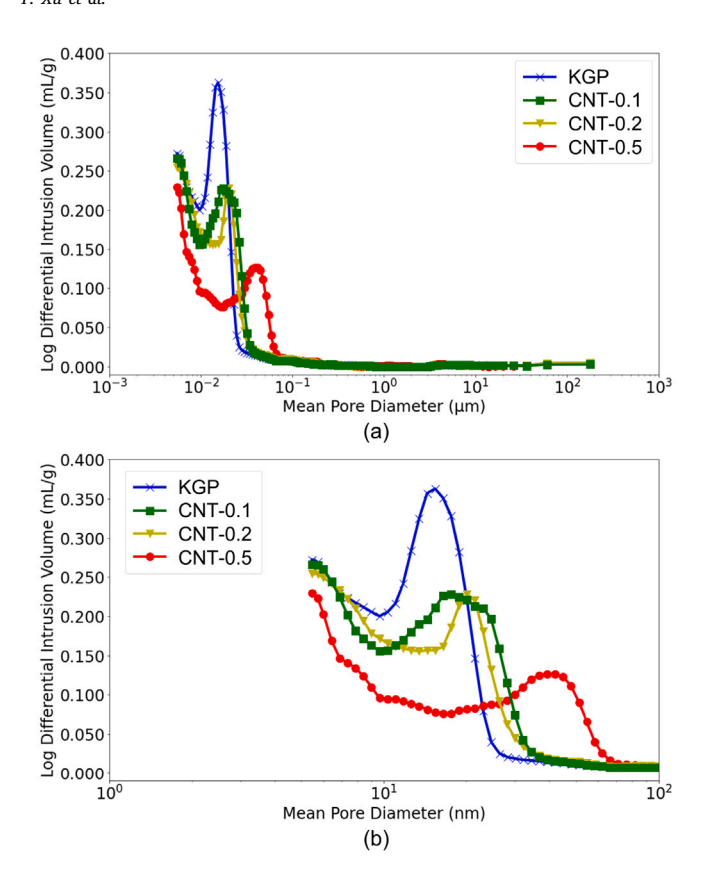


Fig. 6. Log differential pore size distributions for MWCNT-reinforced geopolymer composites: (a) whole range; (b) pore size less than 100 nm.

bond reduces with an increased MWCNT fraction, which indicates a decreased free water concentration resulted from the MWCNTs.

3.3. Porosity characteristics

The porosity characteristics of the geopolymer nanocomposites were analyzed using MIP method. MWCNTs are observed to modify the pore size distributions of metakaolin-based potassium geopolymers at nanoscale, as depicted in Fig. 6. All samples exhibit a clear peak on the log differential intrusion curve. The location of this peak is 15.4 nm, 17.6 nm, 20.1 nm, and 39.2 nm for KGP, CNT-0.1, CNT-0.2, and CNT-0.5, respectively. The value of log differential intrusion at the peak is greatest for pure geopolymer, followed by CNT-0.2, CNT-0.1, and CNT-0.5. For all samples, the log differential intrusion volume is increasing at the smallest recorded mean pore diameter. These results indicate that in metakaolin-based potassium geopolymers, MWCNTs increase the pore diameter at which the first intrusion peak occurs and decrease the magnitude of intrusion at that peak. Moreover, the pore size distributions for the geopolymers show differences only at mean pore diameters below 100 nm (Fig. 6(b)), suggesting that MWCNTs affect the pore structure of potassium geopolymers on a length scale below 100 nm.

Furthermore, MWCNTs affect the pore structure characteristics of metakaolin-based geopolymers, as found in Table 2. The porosity of the pure potassium geopolymer is 23.55%. Compared to this reference sample, concentrations of 0.1%, 0.2%, and 0.5% wt. MWCNTs result in 6.8%, 18.5%, and 26.4% decreases in porosity, respectively. The bulk densities of the samples range from 1.31–1.44 g/cm³, with CNT-0.2 exhibiting the smallest value and CNT-0.5 exhibiting the largest value. Moreover, the skeletal densities range from 1.62–1.79 g/cm³, with CNT-0.2 having the smallest value and CNT-0.1 having the largest value. The threshold pore diameter and water permeability values are

Table 2Pore structure characteristics of pure geopolymer (KGP) and MWCNT-reinforced geopolymer composites.

Sample	Porosity (%)	Bulk Density (g/cm³)	Skeletal Density (g/cm³)	Threshold Pore Diameter (nm)	Water Permeability (m/s)
KGP	23.55	1.36	1.78	22	1.26 x 10 ⁻¹²
CNT-0.1	21.94	1.40	1.79	29	1.44×10^{-12}
CNT-0.2	19.20	1.31	1.62	28	1.18×10^{-12}
CNT-0.5	17.33	1.44	1.74	56	3.16×10^{-12}

affected by MWCNTs. A dosage of 0.1 wt% MWCNTs slightly increases the threshold pore diameter and water permeability, while a dosage of 0.2 wt% slightly increases the threshold pore diameter but decreases the water permeability. 0.2 wt% is an optimum where both the porosity and the threshold pore diameter size are low enough to yield an overall reduction in water permeability: for 0.1wt%, the porosity is too high, whereas for sample 0.5 wt%, the threshold pore diameter is too high. With 0.5 wt% carbon nanotubes, the threshold pore diameter and water permeability are significantly influenced as both values are roughly 2.5 times that of the pure geopolymer. The increase in water permeability correlates with the increase in the peak of the pore size distribution, see Fig. 6. In other words, the MWCNT-induced decrease in porosity is counteracted by an increase in large defects, leading to an increase in water permeability.

3.4. Mechanical properties

MWCNTs result in enhanced long-term creep resistance of the geopolymer composites. The creep modulus and indentation modulus of the MWCNT-reinforced geopolymer composites were obtained from the indentation tests. The histograms of creep modulus of geopolymer composites with different fractions of MWCNTs are displayed in Fig. 7. The histograms of indentation modulus are plotted in the Supplementary Materials document. As the concentration of MWCNTs increases, the distribution of creep modulus expands due to increased heterogeneity of the geopolymer composites. For pure KGP, the mean creep modulus is 24.90 GPa and the median creep modulus is 21.53 GPa. Upon adding 0.1 wt% of MWCNTs, the mean and median creep modulus increase to 34.02 GPa and 28.92 GPa, respectively. A dosage of 0.2 wt% MWCNTs further raises the mean creep modulus to 42.37 GPa and the median creep modulus to 34.60 GPa. CNT-0.5 exhibits a mean creep modulus of 40.90 GPa and a median creep modulus of 34.82 GPa. The addition of MWCNTs resulted in an increased creep modulus of the geopolymer composites. Specifically, the inclusion of 0.2 wt% MWCNTs shows the greatest improvement in the mechanical properties of the geopolymer materials in this study.

In order to further understand the mechanism behind the enhancement of the creep modulus, a phase analysis was performed on the indentation modulus and creep modulus of MWCNT-reinforced geopolymer composites with varying concentrations of MWCNTs, as shown in Fig. 8 where the dominant phase of each composite sample was displayed in red. MWCNTs increase the indentation modulus and creep modulus of the dominant phase. The moduli of each phase were listed in Table S.1 in the Supplementary Materials. For pure geopolymer matrix, the dominant phase is identified to have a volume fraction of 0.35, with corresponding indentation modulus M and creep modulus C values of 7.08 GPa and 20.26 GPa, respectively. In CNT-0.1, the volume fraction of the dominant phase increases to 0.56, with a 18.1% increase in indentation modulus and a 23.6% increase in creep modulus. In CNT-0.2, the volume fraction of the dominant phase further raises to 0.69 and the indentation modulus and creep modulus increase to 9.64 and 35.88 GPa, respectively. For CNT-0.5, the volume fraction of the dominant phase slightly decreases to 0.45. This can be attributed to the fact that a higher dosage of MWCNTs tends to increase the heterogeneity of the composites, as also suggested by the larger variance observed

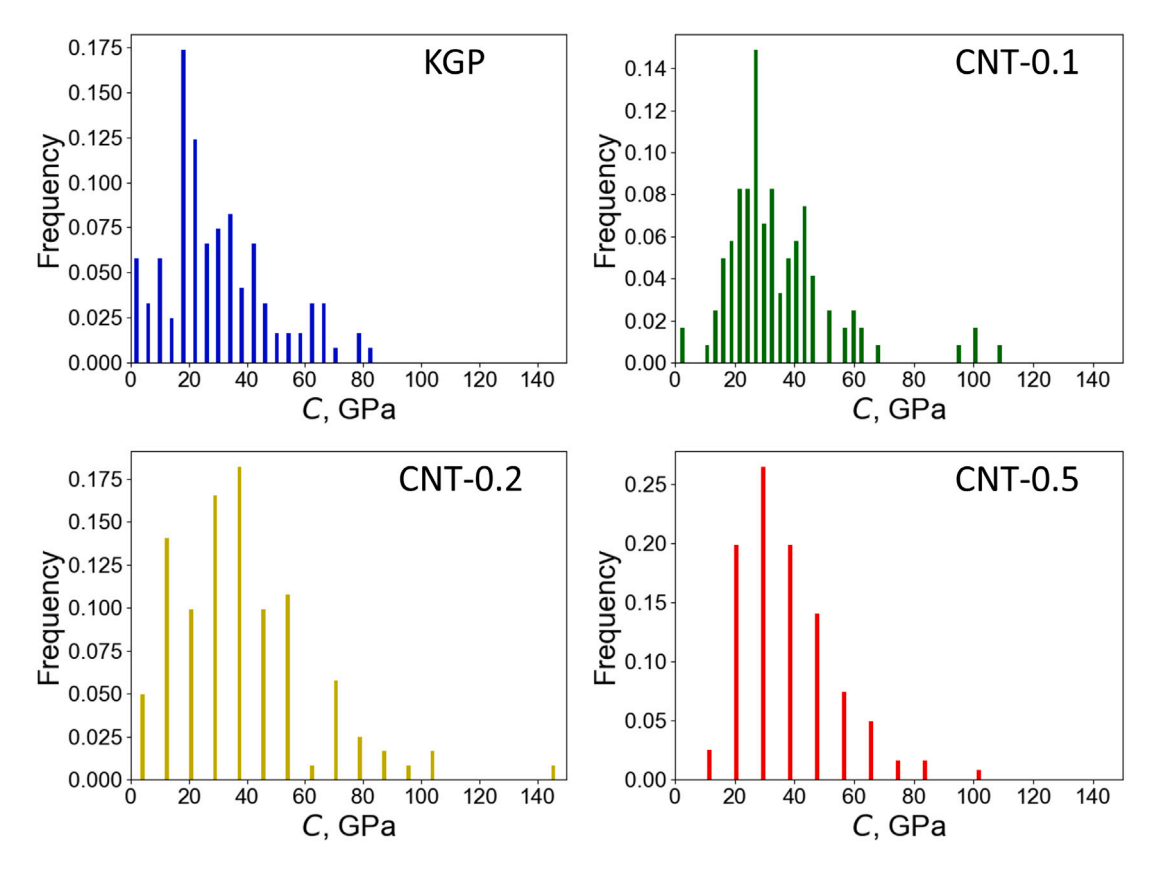


Fig. 7. Histograms of indentation creep modulus of MWCNT-reinforced geopolymer composites.

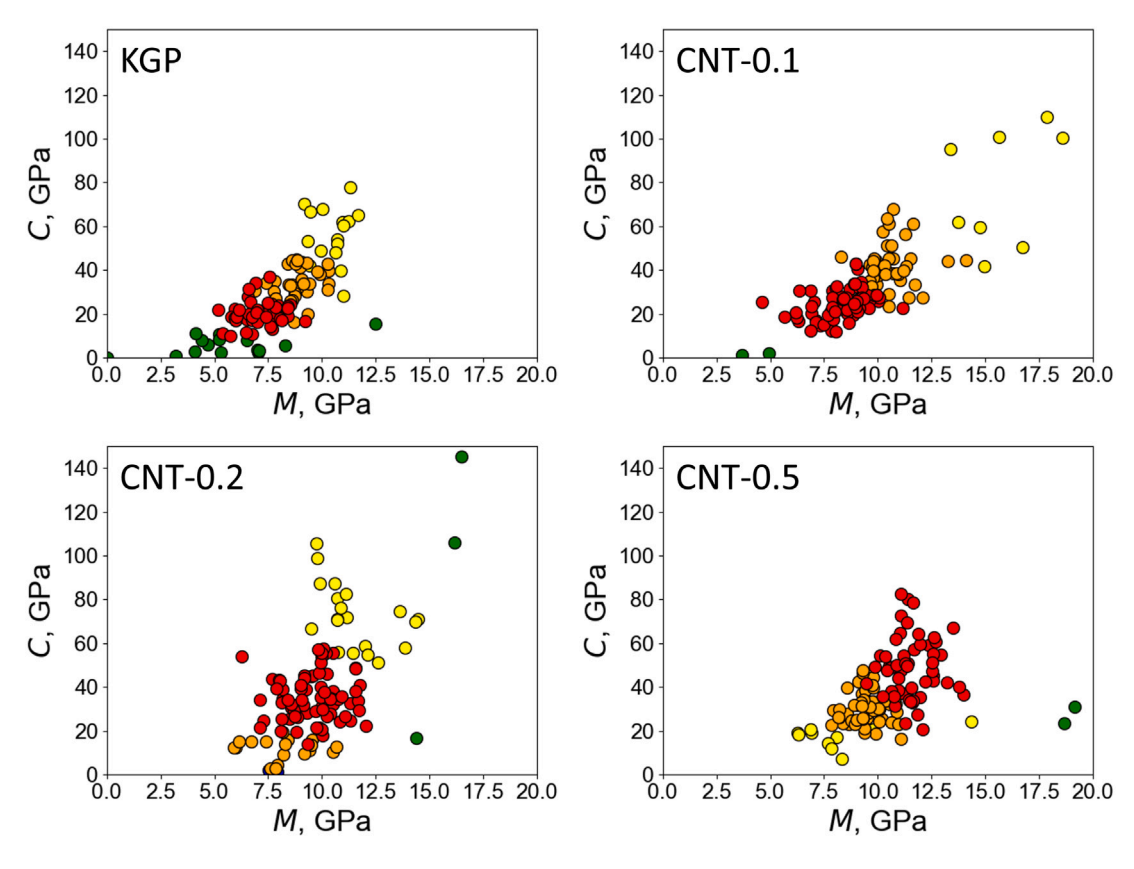
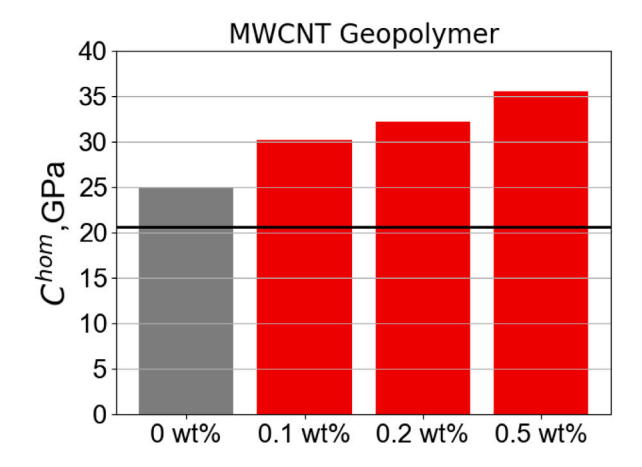


Fig. 8. Phase Analysis of mechanical properties of MWCNT-reinforced geopolymer composites. (For interpretation of the references to color in this figure legend, the reader is referred to the web version of this article.)



 $\textbf{Fig. 9.} \ \ \textbf{Macroscopic creep modulus of MWCNT-reinforced geopolymer composites}.$

in the histograms of creep modulus of CNT-0.5 (Fig. 7). However, the indentation modulus and creep modulus are found to be 11.49 GPa and 48.61 GPa, respectively, for the dominant phase. This leads to a 140% increase in the creep modulus of the dominant phase with the addition of 0.5 wt% of MWCNTs, which demonstrates the significant improvement in the long-term creep resistance induced by MWCNTs.

The macroscopic creep modulus of MWCNT-reinforced geopolymer composites increases with increasing MWCNT fractions, as shown in Fig. 9. For the pure geopolymer matrix with no MWCNTs, the macroscopic creep modulus Chom is 24.96 GPa. With the addition of MWCNTs at concentrations of 0.1 wt%, 0.2 wt%, and 0.5 wt%, the macroscopic creep modulus increases to 30.25 GPa, 32.22 GPa, and 35.51 GPa, respectively. A noticeable increase in Chom with higher concentration of MWCNTs is displayed. Our findings of an increase in macroscopic creep modulus with addition of MWCNTs agree with prior findings in the scientific literature of enhancement in macroscopic mechanical properties such as compressive strength [32,33], flexural strength [33], indentation modulus [5], and fracture toughness [6] with incorporation of carbon-based nanomaterials in geopolymer matrices: however, to our knowledge, our study is the first to look at the creep resistance. The increase in the macroscopic creep modulus is linked to the increase in the creep modulus of the dominant phase. Two mechanisms can potentially explain the increase in the macroscopic creep modulus with increasing fractions of MWCNTs: (i) the MWCNT-induced reduction in porosity due to their catalytic effect, and (ii) the reinforcing mechanism given the high inner strength of MWCNTs which enable them to locally resist long-term deformation. Overall, these results highlight the effectiveness of incorporating MWCNTs as a means to enhance the resilience of geopolymer materials against long-term deformation.

4. Discussion

The experimental results of this study illustrate the possibility of tailoring the architecture of ceramic materials at the nanoscale. In SEM and TEM analysis, a significant integration of MWCNTs and nanoparticulates of geopolymers is observed in the hardened geopolymer composites. MWCNTs act both as a filler and a catalyst. The MWCNTs not only exhibit a crack bridging effect as a nanofiber reinforcement, but they also serve as nucleation sites for geopolymer nanoparticulates during their synthesis process [60]. This can be attributed to the high surface area and surface reactivity of MWCNTs, which promote the geopolymerization reaction. Moreover, the MWCNTs were dispersed in DI water in the first step of geopolymer synthesis, therefore, formed a network within the preceramic precursor in the following steps of the synthesis. This network acts as a hard template that facilitates the self-assembly process in the formation of geopolymer matrix. This

intrinsic templating effect of MWCNTs modifies the architecture of the geopolymer composites.

Furthermore, the increase in the fraction of MWCNTs has been shown to reduce the grain size by 54%, indicating the ability of MWCNTs to tune the nanostructure of the material. The grain size reduction with increase in MWCNT concentration can be explained by considering that the MWCNTs form a mesh that supports geopolymer growth. As the MWCNT concentration increases, the size of the mesh becomes finer, leading to a reduction in grain size. Additionally, MIP measurements have revealed a decrease in porosity by 26% as the fraction of MWCNTs increases to 0.5 wt%, with a drastic change in the pore size distribution within the range of 0–100 nm. This change in pore size distribution is related to the intrinsic porosity of the MWCNTs, acting as hard templates, which has been used to obtain mesoporosity [61,62]. This finding further highlights the ability of MWCNTs to alter the porosity characteristics of the geopolymers at the nanoscale, providing further evidence of their role in tailoring the nanoscale architecture of the ceramic material.

There are two optimal samples, depending on the application. Sample CNT-02 with 0.2 wt% MCWCNTs is optimal for applications that require light-weight properties and durable behavior given the low bulk and skeletal density and the low water permeability. Sample CNT-05 with 0.5 wt% MWCNTs is optimal for applications that require a low porosity and a high resistance to long-term deformation given the low porosity and high values of the macroscopic creep modulus. In other words, multiwalled carbon nanotubes enables us to architect the material to fit the application.

In terms of civil infrastructure applications, the integration of MWC-NTs in metakaolin-based geopolymers leads to an advanced ceramic material that is more resilient to creep propagation and long-term deformation, which is especially preferable in civil infrastructure applications such as bridges. In addition, the advanced MWCNT-reinforced geopolymer nanocomposites can be tailored in terms of their microstructure, pore size distribution and mechanical properties for specific application purposes, such as green cement [63,64], waste treatment [65,66], and heavy metal containment [67]. In brief, the findings in this study provide valuable insights in the development of next-generation smart geopolymer-based civil engineering materials using carbon-based nanomaterials.

5. Conclusions

The original scientific question was how to tailor the architecture of nanostructured ceramics such as geopolymers using MWCNTs. Below are our major findings:

- SEM and TEM imaging reveal that multiwalled carbon nanotubes (MWCNTs) template the structure of geopolymers at the nanoscale. They fill micropores and bridge microcracks. Geopolymer nanoparticles growth is observed along the walls of MWCNTs. Increasing the fraction of MWCNTs by 0.5 wt% leads to a reduction in grain size by 54%.
- X-ray diffraction shows MWCNTs preserve the amorphous structure of geopolymers and promote the reaction between the raw materials. FTIR further reveals the formation of a denser structure facilitated by MWCNTs.
- MIP shows that MWCNTs lead to a drastic change in pore size distribution from a single dominant peak to a lowered diffusive peak. The incorporation of MWCNTs leads to a shift in the second peak of the log differential intrusion curve. Overall, the pore size remain below 100 nm; still, a 26% decrease in porosity is observed as the fraction of MWCNTs is increased to 0.5 wt%.
- Creep indentation shows both a local and global stiffening. As
 the fraction of MWCNTs increases, both the indentation modulus
 and logarithmic creep indentation modulus of the dominant phase
 increase. At the macroscopic level, the macroscopic logarithmic creep modulus is 42% higher in CNT-0.5 than that of pure
 geopolymer.

Overall, our results show that owing to the self-assembly process of geopolymers and the templating mechanism of carbon nanotubes, MWCNT-reinforced geopolymers are architected ceramic nanocomposites with a tunable nanoscale porosity and grain size, as well as enhanced mechanical properties.

Declaration of competing interest

The authors declare that they have no known competing financial interests or personal relationships that could have appeared to influence the work reported in this paper.

Data availability

Data will be made available on request.

Acknowledgments

This work was supported by the National Science Foundation, United States under grant number DMR 1928702. This work was supported by the National Science Foundation, United States under Grant No. 1747452, which supported Nathanial Buettner in his Ph.D. studies. This work made use of the EPIC facility of Northwestern University's NUANCE Center, which has received support from the Soft and Hybrid Nanotechnology Experimental (SHyNE) Resource, United States (NSF ECCS-1542205); the MRSEC program (NSF DMR-1720139) at the Materials Research Center; the International Institute for Nanotechnology (IIN), United States; the Keck Foundation, United States; and the State of Illinois, United States, through the IIN.

Appendix A. Supplementary data

Supplementary material related to this article can be found online at https://doi.org/10.1016/j.mechrescom.2023.104216.

References

- [1] J.L. Provis, P. Duxson, J.S. van Deventer, The role of particle technology in developing sustainable construction materials, Adv. Powder Technol. 21 (1) (2010) 2-7.
- [2] P. Moriarty, Nanostructured materials, Rep. Progr. Phys. 64 (3) (2001) 297.
- [3] Y. Hu, D. Ye, B. Luo, H. Hu, X. Zhu, S. Wang, L. Li, S. Peng, L. Wang, A binder-free and free-standing cobalt sulfide@ carbon nanotube cathode material for aluminum-ion batteries, Adv. Mater. 30 (2) (2018) 1703824.
- [4] D. Ji, L. Fan, L. Li, S. Peng, D. Yu, J. Song, S. Ramakrishna, S. Guo, Atomically transition metals on self-supported porous carbon flake arrays as binder-free air cathode for wearable zinc-air batteries, Adv. Mater. 31 (16) (2019) 1808267.
- [5] J. Chen, A.T. Akono, Influence of multi-walled carbon nanotubes on the fracture response and phase distribution of metakaolin-based potassium geopolymers, J. Mater. Sci. 56 (2021) 19403–19424.
- [6] A.T. Akono, Fracture behavior of Metakaolin-based geopolymer reinforced with carbon nanofibers, Int. J. Ceram. Eng. Sci. 2 (5) (2020) 234–242.
- [7] Y. Wang, T. Yokota, T. Someya, Electrospun nanofiber-based soft electronics, NPG Asia Mater. 13 (1) (2021) 22.
- [8] B. Wang, A. Thukral, Z. Xie, L. Liu, X. Zhang, W. Huang, X. Yu, C. Yu, T.J. Marks, A. Facchetti, Flexible and stretchable metal oxide nanofiber networks for multimodal and monolithically integrated wearable electronics, Nat. Commun. 11 (1) (2020) 2405.
- [9] M. Fan, C. Zhu, J. Yang, D. Sun, Facile self-assembly N-doped graphene quantum dots/graphene for oxygen reduction reaction, Electrochim. Acta 216 (2016) 102–109.
- [10] D.M. Kroupa, G.F. Pach, M. Voros, F. Giberti, B.D. Chernomordik, R.W. Crisp, A.J. Nozik, J.C. Johnson, R. Singh, V.I. Klimov, G. Galli, Enhanced multiple exciton generation in PbS, CdS Janus-like heterostructured nanocrystals, ACS Nano 12 (10) (2018) 10084–10094.
- [11] X. Han, X. Ling, D. Yu, D. Xie, L. Li, S. Peng, C. Zhong, N. Zhao, Y. Deng, W. Hu, Atomically dispersed binary Co-Ni sites in nitrogen-doped hollow carbon nanocubes for reversible oxygen reduction and evolution, Adv. Mater. 31 (49) (2019) 1905622.
- [12] A.P. Singh, A. Biswas, A. Shukla, P. Maiti, Targeted therapy in chronic diseases using nanomaterial-based drug delivery vehicles, Signal Transduct. Targeted Therapy 4 (1) (2019) 33.

- [13] M. Elsabahy, K.L. Wooley, Design of polymeric nanoparticles for biomedical delivery applications, Chem. Soc. Rev. 41 (7) (2012) 2545–2561.
- [14] V. Brahmkhatri, P. Pandit, P. Rananaware, A. D'Souza, M.D. Kurkuri, Recent progress in detection of chemical and biological toxins in water using plasmonic nanosensors, Trends Environ. Analyt. Chem. 30 (2021) e00117.
- [15] A.A. Beni, A. Esmaeili, Design and optimization of a new reactor based on biofilm-ceramic for industrial wastewater treatment, Environ. Pollut. 255 (2019) 113298.
- [16] J.K.Y. Lee, N. Chen, S. Peng, L. Li, L. Tian, N. Thakor, S. Ramakrishna, Polymer-based composites by electrospinning: Preparation & functionalization with nanocarbons, Prog. Polym. Sci. 86 (2018) 40–84.
- [17] D. Nepal, S. Kang, K.M. Adstedt, K. Kanhaiya, M.R. Bockstaller, L.C. Brinson, M.J. Buehler, P.V. Coveney, K. Dayal, J.A. El-Awady, L.C. Henderson, Hierarchically structured bioinspired nanocomposites, Nat. Mater. 22 (1) (2023) 18–35.
- [18] W.M. Kriven, M. Gordon, J.L. Bell, Geopolymers: Nanoparticulate, nanoporous ceramics made under ambient conditions, Microsc. Microanal. 10 (S02) (2004) 404–405.
- [19] J.L. Bell, W.M. Kriven, Nanoporosity in aluminosilicate, geopolymeric cements, Microsc. Microanal. 10 (S02) (2004) 590–591.
- [20] W.M. Kriven, J.L. Bell, S.W. Mallicoat, M. Gordon, Intrinsic microstructure and properties of metakaolin-based geopolymers, in: International Worshop on Geopolymer Binders: Interdependence of Composition, Structure and Properties, 2007, pp. 71–86.
- [21] J. Davidovits, Geopolymers: Ceramic-like inorganic polymers, J. Ceram. Sci. Technol. 8 (3) (2017) 335–350.
- [22] J.J. Bowen, L.M. Rueschhoff, K.L. Martin, D.P. Street, T.A. Patel, M.J. Parvulescu, N.M. Bedford, H. Koerner, S. Seifert, M.B. Dickerson, Tailorable micelle morphology in self-assembling block copolymer gels for templating nanoporous ceramics, Macromolecules 53 (17) (2020) 7528–7536.
- [23] J. Davidovits, Geopolymer-Chemistry and Applications, Geopolymere Institute, Saint-Quentin, France, 2008, pp. 63–422.
- [24] K. Baek, I. Hwang, I. Roy, D. Shetty, K. Kim, Self-assembly of nanostructured materials through irreversible covalent bond formation, Account. Chem. Res. 48 (8) (2015) 2221–2229.
- [25] K. Oh, H. Yi, R. Kou, Y. Qiao, Compaction self-assembly of a low-binder-content geopolymer material, J. Mater. Sci. 55 (2020) 15397–15404.
- [26] Z. Lao, Y. Hu, C. Zhang, L. Yang, J. Li, J. Chu, D. Wu, Capillary force driven self-assembly of anisotropic hierarchical structures prepared by femtosecond laser 3D printing and their applications in crystallizing microparticles, Acs Nano. 9 (12) (2015) 12060–12069.
- [27] W.M. Kriven, J.L. Bell, M. Gordon, Microstructure and microchemistry of fully-reacted geopolymers and geopolymer matrix composites, Ceram. Trans. 153 (1994) (2003) 227–250.
- [28] N. Shehata, O.A. Mohamed, E.T. Sayed, M.A. Abdelkareem, A.G. Olabi, Geopolymer concrete as green building materials: Recent applications, sustainable development and circular economy potentials, Sci. Total Environ. (2022) 155577.
- [29] N. Dave, V. Sahu, A.K. Misra, Development of geopolymer cement concrete for highway infrastructure applications, J. Eng. Des. Technol. 18 (5) (2020) 1321–1333.
- [30] A.M. Aguirre-Guerrero, R.M. de Gutiérrez, Alkali-activated protective coatings for reinforced concrete exposed to chlorides, Constr. Build. Mater. 268 (2021) 121008
- [31] A. Drabczyk, S. Kudłacik-Kramarczyk, K. Korniejenko, B. Figiela, G. Furtos, Review of geopolymer nanocomposites: Novel materials for sustainable development, Materials 16 (9) (2023) 3478.
- [32] S.M. Abbasi, H. Ahmadi, G. Khalaj, B. Ghasemi, Microstructure and mechanical properties of a metakaolinite-based geopolymer nanocomposite reinforced with carbon nanotubes, Ceram. Int. 42 (14) (2016) 15171–15176.
- [33] G. da Luz, P.J.P. Gleize, E.R. Batiston, F. Pelisser, Effect of pristine and functionalized carbon nanotubes on microstructural, rheological, and mechanical behaviors of metakaolin-based geopolymer, Cement Concrete Compos. 104 (2019) 103332.
- [34] S. Zhang, C. Wang, Precise analysis of nanoparticle size distribution in TEM image, Methods Protocols 6 (4) (2023) 63.
- [35] N. El Horr, Z. Valdez-Nava, C. Tenailleau, S. Guillemet-Fritsch, Microstructure of Ba1xLaxTiO3 δ ceramics sintered by spark plasma sintering, J. Eur. Ceram. Soc. 31 (6) (2011) 1087–1096.
- [36] S.O. Gashti, A. Fattah-Alhosseini, Y. Mazaheri, M.K. Keshavarz, Effects of grain size and dislocation density on strain hardening behavior of ultrafine grained AA1050 processed by accumulative roll bonding, J. Alloys Compd. 658 (2016) 854–861.
- [37] B.H. O'Connor, W.J. Chang, The amorphous character and particle size distributions of powders produced with the micronizing mill for quantitative x-ray powder diffractometry, X-ray Spectromet. 15 (4) (1986) 267–270.
- [38] V.J. Hurst, P.A. Schroeder, R.W. Styron, Accurate quantification of quartz and other phases by powder X-ray diffractometry, Anal. Chim. Acta 337 (3) (1997) 233–252.
- [39] S.S. Musil, W.M. Kriven, In situ mechanical properties of chamotte particulate reinforced, potassium geopolymer, J. Am. Ceram. Soc. 97 (3) (2014) 907–915.

- [40] J.L. Bell, P.E. Driemeyer, W.M. Kriven, Formation of ceramics from metakaolin-based geopolymers, part II: K-based geopolymer, J. Am. Ceram. Soc. 92 (3) (2009) 607–615
- [41] A.B. Abell, K.L. Willis, D.A. Lange, Mercury intrusion porosimetry and image analysis of cement-based materials, J. Colloid Interface Sci. 211 (1) (1999) 39–44.
- [42] P.A. Webb, An introduction to the physical characterization of materials by mercury intrusion porosimetry with emphasis on reduction and presentation of experimental data, Micromeritics Instrument Corp, Norcross, Georgia, 2001.
- [43] H. Ma, Mercury intrusion porosimetry in concrete technology: Tips in measurement, pore structure parameter acquisition and application, J. Porous Mater. 21 (2014) 207–215.
- [44] A.J. Katz, A.H. Thompson, Prediction of rock electrical conductivity from mercury injection measurements, J. Geophys. Res.: Solid Earth 92 (B1) (1987) 599-607
- [45] W.C. Oliver, G.M. Pharr, An improved technique for determining hardness and elastic modulus using load and displacement sensing indentation experiments, J. Mater. Res. 7 (6) (1992) 1564–1583.
- [46] M. Vandamme, F.J. Ulm, Viscoelastic solutions for conical indentation, Int. J. solids struct. 43 (10) (2006) 3142–3165.
- [47] M. Vandamme, F.J. Ulm, Nanoindentation investigation of creep properties of calcium silicate hydrates. Cem. Concr. Res. 52 (2013) 38–52.
- [48] G. Constantinides, K.R. Chandran, F.J. Ulm, K.J. Van Vliet, Grid indentation analysis of composite microstructure and mechanics: Principles and validation, Mater. Sci. Eng. A 430 (1–2) (2006) 189–202.
- [49] A.T. Akono, G. Dávila, J. Druhan, Z. Shi, K. Jessen, T. Tsotsis, Influence of geochemical reactions on the creep behavior of Mt. Simon sandstone, Int. J. Greenh. Gas Control 103 (2020) 103183.
- [50] G. Cowan, Statistical Data Analysis, Oxford university press, 1998.
- [51] H. Ahmadi, G. Khalaj, A. Najafi, S.M. Abbasi, M. Safari, Metakaolin-red mud/carbon nanotubes geopolymer nanocomposite: Mechanical properties and structural studies, Mater. Res. Express 9 (2) (2022) 025011.
- [52] P.S.W.M. Duxson, S.W. Mallicoat, G.C. Lukey, W.M. Kriven, J.S. Van Deventer, The effect of alkali and Si/Al ratio on the development of mechanical properties of metakaolin-based geopolymers, Colloids Surf. A 292 (1) (2007) 8–20.
- [53] Z. Li, Q. Fan, Y. Yin, Colloidal self-assembly approaches to smart nanostructured materials, Chem. Rev. 122 (5) (2021) 4976–5067.
- [54] L. Zhang, L. Jin, B. Liu, J. He, Templated growth of crystalline mesoporous materials: From soft/hard templates to colloidal templates, Front. Chem. 7 (22) (2019).

- [55] J. Davidovits, Properties of geopolymer cements, in: First International Conference on Alkaline Cements and Concretes. Vol. 1, 1994, pp. 131–149.
- [56] Z. Zidi, M. Ltifi, I. Zafar, Synthesis and attributes of nano-SiO2 local metakaolin based-geopolymer, J. Build. Eng. 33 (2021) 101586.
- [57] P. Rovnanik, Effect of curing temperature on the development of hard structure of metakaolin-based geopolymer, Construct. Buil. Mater. 24 (7) (2010) 1176–1183.
- [58] C.A. Rees, J.L. Provis, G.C. Lukey, J.S. Van Deventer, In situ ATR-FTIR study of the early stages of fly ash geopolymer gel formation, Langmuir 23 (17) (2007) 9076–9082
- [59] P. Innocenzi, Infrared spectroscopy of sol-gel derived silica-based films: A spectra-microstructure overview, J. Non-Crystall. Solids 316 (2-3) (2003) 309-319
- [60] A. Akbar, K.M. Liew, F. Farooq, R.A. Khushnood, Exploring mechanical performance of hybrid MWCNT and GNMP reinforced cementitious composites, Constr. Build. Mater. 267 (2021) 120721.
- [61] J.Y. Cheng, C.A. Ross, H.I. Smith, E.L. Thomas, Templated self-assembly of block copolymers: Top-down helps bottom-up, Adv. Mater. 18 (19) (2006) 2505–2521.
- [62] A.F. Sierra-Salazar, A. Ayral, T. Chave, V. Hulea, S.I. Nikitenko, S. Abate, S. Perathoner, P. Lacroix-Desmazes, Unconventional pathways for designing silica-supported Pt and Pd catalysts with hierarchical porosity, in: Studies in Surface Science and Catalysis. Vol. 178, Elsevier, 2019, pp. 377–397.
- [63] P. Duxson, J.L. Provis, G.C. Lukey, J.S. Van Deventer, The role of inorganic polymer technology in the development of 'green concrete', Cement Concrete Res. 37 (12) (2007) 1590–1597.
- [64] M. Sandanayake, C. Gunasekara, D. Law, G. Zhang, S. Setunge, D. Wanijuru, Sustainable criterion selection framework for green building materials—an optimisation based study of fly-ash geopolymer concrete, Sustain. Mater. Technol. 25 (2020) e00178.
- [65] I. Luhar, S. Luhar, M.M.A.B. Abdullah, R.A. Razak, P. Vizureanu, A.V. Sandu, P.D. Matasaru, A state-of-the-art review on innovative geopolymer composites designed for water and wastewater treatment, Materials 14 (23) (2021) 7456.
- [66] C.J. Li, Y.J. Zhang, H. Chen, P.Y. He, Q. Meng, Development of porous and reusable geopolymer adsorbents for dye wastewater treatment, J. Clean. Prod. 348 (2022) 131278.
- [67] A. Maleki, Z. Hajizadeh, V. Sharifi, Z. Emdadi, A green, porous and ecofriendly magnetic geopolymer adsorbent for heavy metals removal from aqueous solutions. J. Clean. Prod. 215 (2019) 1233–1245.